Structure, microstructure and electrical conductivity of 8YSZ containing NiO

R.M. Batista, E.N.S. Muccillo *

Energy and Nuclear Research Institute-CCTM, Av. Prof. Lineu Prestes, 2242, Cidade Universitária, S. Paulo, 05508-000, SP, Brazil

Abstract

The effects of NiO addition on the structure and microstructure of yttria-stabilized zirconia were investigated to clarify the role of the additive in the microstructure-related electrical conductivity of the solid electrolyte. Specimens of 8 mol% yttria-stabilized zirconia with NiO contents up to 5.0 mol% were prepared using nickel oxide and trihydroxi nickel carbonate as precursors. The specimens were sintered at 1350 °C for several holding times. The evolution of the lattice parameter with NiO content was evaluated by X-ray diffraction and the microstructural features by scanning electron microscopy. Electrical conductivity was evaluated by impedance spectroscopy measurements. The solubility limit of NiO at 1350 °C was found to be 1.5 mol% by X-ray diffraction. Energy dispersive spectroscopy results revealed Ni segregation for large holding times at 1350 °C. The grain boundary conductivity was found to be influenced by Ni segregation and to decrease with increasing holding times at high temperature.
© 2011 Elsevier Ltd and Techna Group S.r.l. All rights reserved.

1. Introduction

Solid oxide fuel cells (SOFCs) are electrochemical devices that convert chemical energy into electrical energy. SOFCs show many advantages compared to traditional energy generation systems, such as high efficiency, fuel flexibility, modularity, and low SOx and NOx emissions [1].

Many investigations in the field of high-temperature solid oxide fuel cells have focused on development of appropriate materials, but the most frequently used are still yttria-stabilized zirconia (YSZ), the Ni/YSZ cermet and lanthanum strontium manganite (LSM) as solid electrolyte, anode and cathode, respectively [2].

In general, nickel oxide and zirconia containing 8 mol% yttria (8YSZ) are employed as starting materials for manufacturing the SOFCs anode. These precursors are mixed together and thermally treated at high temperature (> 1000 °C). During this thermal treatment, dissolution of NiO may occur. In a previous study, it has been shown that the activation energy for the solid solution formation is as low as 0.25 eV [3].

The NiO solid solubility in partially stabilized zirconia (5 and 6 mol% Y$_2$O$_3$) was reported to be lower than 3 mol% at 1300 °C [4]. In a subsequent study, the solubility of nickel oxide into 8YSZ was proposed to be maximized in the 1200 to 1600 °C range, and estimated to amount 1.4 mol% [5].

The effect of nickel oxide on the electrical conductivity of yttria-stabilized zirconia has also been the subject of various investigations. Electrical conductivity lowering with nickel oxide addition to 8YSZ was observed by Linderoth et al. [6]. This effect was attributed to Ni precipitates, which were formed during the reduction reaction of NiO. Moreover, the additive resulted in a decreased initial conductivity (as-sintered) of the solid electrolyte. Van Herle and Vasquez [7] obtained a similar degradation of the electrical conductivity of 8YSZ, but did not observe any effect of NiO in the initial conductivity. In contrast, Coors [8] reported a slight increase in the initial conductivity of stabilized zirconia due to nickel oxide addition.

In this work, NiO was used as a sintering aid and the effects on the structure, microstructure and electrical conductivity of 8YSZ were systematically investigated. The main purposes were to determine experimentally the solubility limit of the

* Corresponding author. Tel.: +55 11 31339203; fax: +55 11 31339276.
E-mail address: enavarro@usp.br (E.N.S. Muccillo).

additive at a typical sintering temperature, and to clarify its role on grain and grain boundary conductivities of the solid electrolyte.

2. Experimental

2.1. Powder materials and processing

Zirconia-8 mol% yttria (99.6%, Tosoh), NiO (99%, Alfa Aesar) and $NiCO_3.3Ni(OH)_2.xH_2O$ (99.5%, Alfa Aesar) commercial powders were used as-received. Specimens prepared with nickel oxide and trihydroxi nickel carbonate precursors will be denoted NO and NC, respectively.

Additions of 0.5 to about 5 mol% of NiO to 8YSZ were carried out by mechanical mixing. The starting materials were mixed together in selected proportions in alcoholic medium for 1 h using zirconia balls. Cylindrical specimens were prepared by uniaxial pressing followed by sintering in air at 1350 °C for holding times varying from 0.1 to 15 h. Green compacts prepared by the mixture of 8YSZ and trihydroxi nickel carbonate were first heated to 600 °C for 10 min to allow for decomposition of the precursor material, and then heated up to the sintering temperature.

2.2. Characterization methods

X-ray diffraction (XRD) analysis was performed using a diffractometer (Bruker-AXS, D8 Advance) in a Bragg-Brentano configuration, with a Ni-filtered Cu K_α radiation in the 25 to 97° 2θ range operating at 40 kV and 30 mA. Lattice parameters were determined using high-grade Si as an internal standard. At least two independent determinations were carried out for each composition. Selected specimens were observed in a scanning electron microscope (Philips, XL30) using secondary electrons. The mean grain size, G, of the sintered specimens was calculated by the intercept method in a population of about 1000 grains. Additional microstructure characterization was carried out by energy dispersive spectroscopy (EDS) coupled to a field emission scanning electron microscope, FE-SEM (Jeol, JSM 670 1F). Electrical conductivity of sintered specimens was determined by impedance spectroscopy measurements in a low-frequency analyzer (HP 4192A). Silver paste was applied by painting onto the large surfaces of specimens and fired at 400 °C for 15 minutes to act as electrode material. Resistance data were collected in the 5 Hz-13 MHz frequency range under 100 mV ac signal.

3. Results and discussion

3.1. Structure and microstructure

The structural characterization was carried out on specimens sintered at 1350 °C for 5 h. Fig. 1 shows a typical X-ray diffraction pattern obtained for 8YSZ. The cubic fluorite-type structure (space group *Fm3m*) of zirconia was indexed according to JCPDS file 30-1468. Small displacements in 2θ, and broadening of the full width at half maximum of
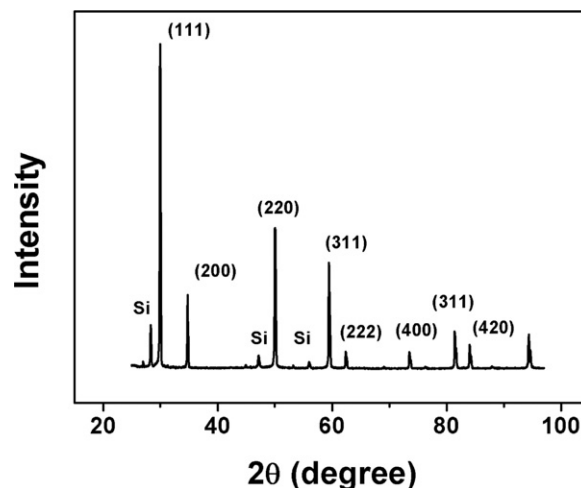
Fig. 1. X-ray diffraction pattern of 8YSZ sintered at 1350 °C for 5 h. Si was used as a standard.

diffraction peaks were observed for specimens containing NiO. Three peaks of the standard material may be also observed in this figure.

Lattice parameters were determined from X-ray diffraction patterns by the extrapolation method against $\cos^2\theta$ [9]. To avoid any interference, mostly due to trace amounts of tetragonal phase usually present on the surface of sintered specimens, the most intense crystalline planes ((111) and (220)) were neglected in this analysis. Fig. 2 shows the calculated lattice parameters as a function of the NiO content.

The lattice parameter of cubic stabilized zirconia decrease linearly with increasing NiO contents up to 1.5 mol%, and reach a steady state regime above that concentration. This means that Ni^{2+} is incorporated into the zirconia lattice forming a substitutional solid solution and the corresponding variation of the lattice parameter follows the Vegard's law. The maximum solubility of Ni^{2+} at 1350 °C is about 1.5 mol%, and beyond that value the additive remains as NiO (cubic, NaCl-type), as revealed by Raman spectroscopy [10].

Fig. 3 shows typical scanning electron microscopy micrographs of (a) 8YSZ, and 8YSZ with x mol% NiO using (b)
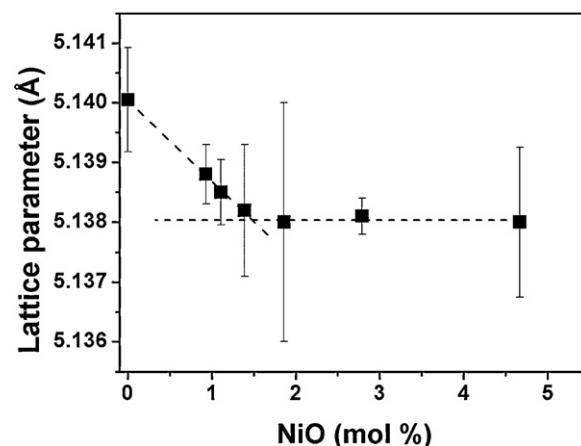
Fig. 2. Evolution of the lattice parameter of 8YSZ with NiO content determined by XRD analysis.
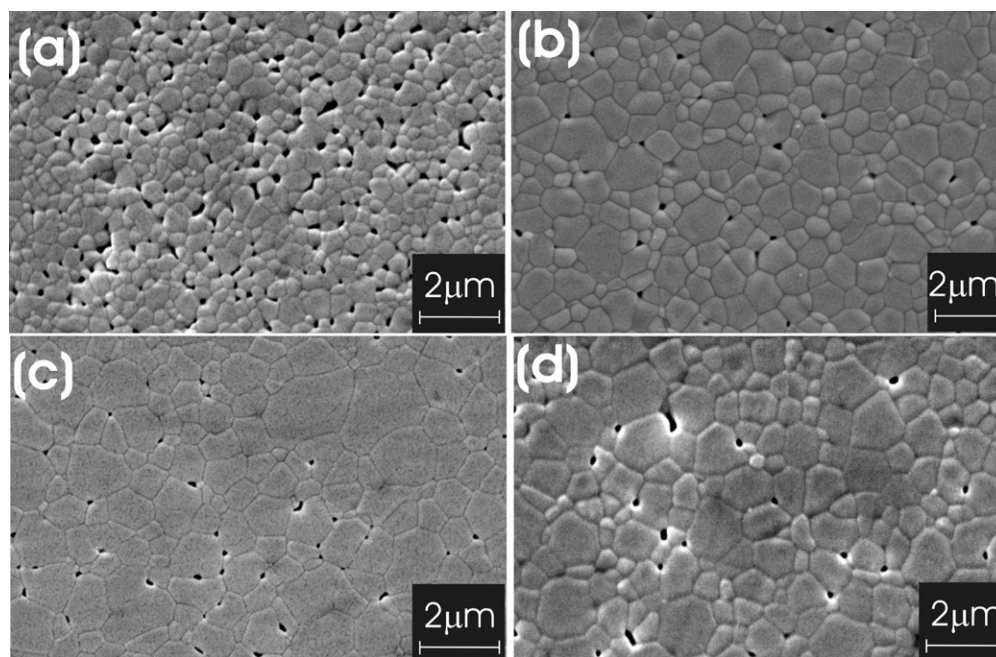
Fig. 3. Scanning electron microscopy micrographs of (a) 8YSZ and 8YSZ specimens containing x mol% NiO prepared with (b) nickel oxide (x = 0.5), (c) nickel carbonate (x = 0.5) and (d) nickel carbonate (x = 1.0). Sintering conditions: 1350 °C for 0.1 h.

nickel oxide (x = 0.5), (c) nickel carbonate (x = 0.5) and (d) nickel carbonate (x = 1.0) as precursors. Sintering conditions were 1350 °C and 0.1 h. No heterogeneities can be observed on the micrographs.

The main differences in the microstructure of the sintered ceramics are the mean grain size and the residual porosity. Specimens containing NiO exhibit enhanced grain growth and improved densification rate in the intermediate stage of sintering [11]. This is an additional evidence of a solid solution formation, even for short holding times. These results are in general agreement with those of Kuzjukevics and Linderoth [3].

The evolution of the mean grain size with the holding time at 1350 °C for specimens with different amounts of NiO and prepared with different nickel precursors is shown in Fig. 4.
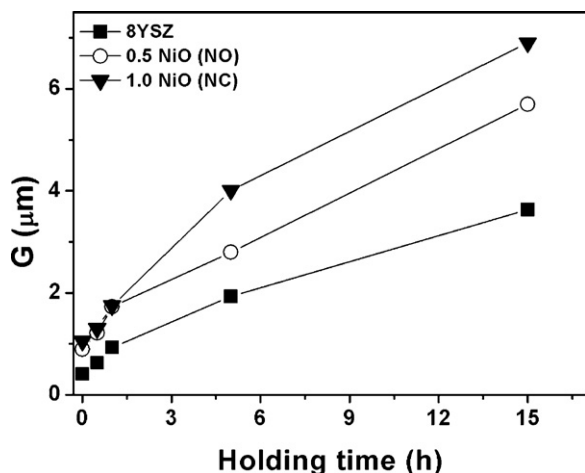
Whatever the experimental conditions, specimens containing NiO show higher average grain size compared to pure 8YSZ. After 5 h at 1350 °C, for example, the average grain size of 8YSZ is 1.9 μm and that of 8YSZ containing 1 mol% NiO is 4.0 μm.

The effect of increasing the holding time on the microstructure of the pure 8YSZ specimens was to increase the grain size. No other effect was observed in specimens sintered up to 15 h at 1350 °C.

In contrast, a secondary phenomenon occurred in specimens containing NiO, as revealed by scanning electron microscopy, where few microregions exhibit "holes". The medium grain size is about 6.9 μm for specimens (1.0 mol% NiO-NC) sintered at 1350 °C for 15 h. These "holes" may not be attributed to grain pullout. The morphology of these specific microregions consists of regular grains surrounded by relatively small grains.

The EDS analysis was performed few micrometers underneath the specimen surface (after polishing with sandpaper of 600 mesh) on randomly chosen points. The relative contents of Zr, Y and Ni are listed in Table 1.

Fig. 4. Average grain size versus holding time of pure 8YSZ and 8YSZ containing NiO specimens.

Table 1
Semiquantitative analysis of Ni, Y and Zr in specific regions of a 0.5 mol% NiO specimen sintered at 1350 °C for 15 h.

Microregion	Ni (at.%)	Y (at.%)	Zr (at.%)
1	1.15	13.34	85.51
2	0.70	13.97	85.33
3	1.42	12.94	85.64
4	0.48	13.28	86.24
5	0.00	11.82	88.18
6	95.58	0.55	3.87

It is worth noting the non uniform Ni distribution in regions denoted 1 to 5 (Table 1), whereas the relative Y and Zr contents are the same within experimental errors. Region 6 corresponds to a high Ni content grain while keeping constant Y/Zr ratio. This high Ni content evidences a segregation effect resulting from nickel diffusion at high temperatures and over long holding times.

Similar effects on the microstructure of sintered specimens were observed independently of the type of nickel precursor and NiO content. The segregation of the additive depends on holding time and temperature. At 1350 °C this effect was detected for holding times longer than 5 h. This microstructural effect is expected to result in a degradation of the electrical conductivity and mechanical properties of 8YSZ.

3.2. Electrical conductivity

Arrhenius plots of the overall electrolyte conductivity, σ, are plotted in Fig. 5 for selected specimens with similar relative density (97-98% of the theoretical density). Specimens containing NiO were sintered at 1350 °C for 1 h, whereas for pure 8YSZ the holding time was 5 h. The grain sizes varied from 1.40 μm (0.5 mol% NiO - NC) to 1.95 μm (8YSZ).

In the restricted temperature range of measurements the Arrhenius plots exhibit a simple behavior. The straight lines are fairly parallel to each other and the apparent activation energy is 1.12 ± 0.03 eV. Specimens prepared with nickel oxide precursor and 8YSZ without additive show a slightly higher electrical conductivity compared to other specimens. This effect may result from different impurities in the precursor materials and/or incomplete decomposition of the trihydroxy nickel carbonate. It is worth noting the identical electrical conductivity behavior of pure 8YSZ and NiO-containing 8YSZ specimens prepared with nickel oxide. Then, it may be concluded that the overall electrolyte conductivity is independent on NiO contents up to 1.0 mol% (near its solubility limit). The differences observed in previous works may be related to impurities (type and relative contents) in the precursor of the additive material.
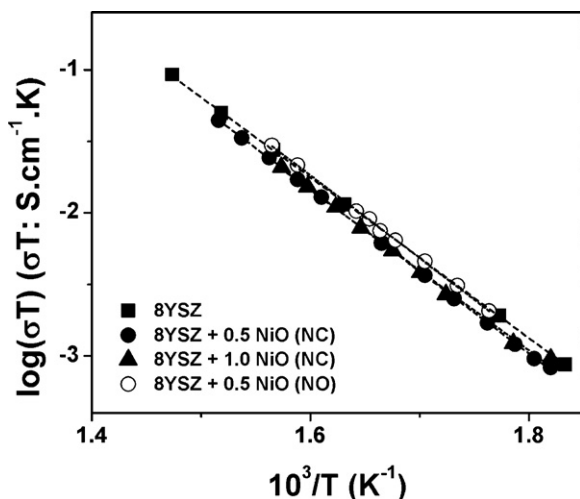
Fig. 5. Arrhenius plots of the overall electrolyte conductivity of specimens with similar density (97–98% of the theoretical value).
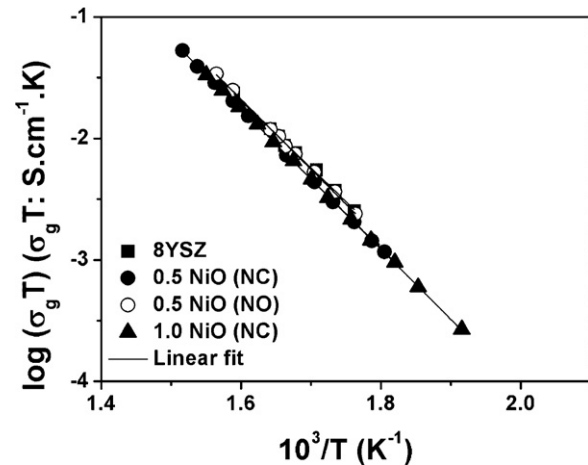
Fig. 6. Arrhenius plots of the electrical conductivity of grains of the same specimens shown in Fig. 7.

Arrhenius plots of the intragrain electrical conductivity, σ_g, for the same specimens are shown in Fig. 6.

The grain conductivity of all studied specimens is of the same order of magnitude. Slightly higher grain conductivity is found for pure 8YSZ and 8YSZ containing 0.5 mol% NiO prepared with nickel oxide. Apparent activation energy values are 1.10 (8YSZ), and 1.14 eV (NiO containing specimens).

Fig. 7 shows Arrhenius plots for the grain boundary conductivity, σ_{gb}, of (a) pure 8YSZ and (b) 8YSZ containing 1 mol% NiO as a function of the holding time at 1350 °C.

The grain boundary conductivity of 8YSZ, (Fig. 7a), increases steadily with increasing the holding time, in other words, with increasing grain size (or decreasing the grain boundary surface). The fitted straight lines show a parallel behavior evidencing that no changes occur in the conductivity mechanism.

The behavior of the grain boundary conductivity of 8YSZ containing NiO (Fig. 7b) remains similar to that of 8YSZ for short holding times, except that the increase in the magnitude of conductivity with holding time is smaller in this case. After 15 h at 1350 °C the conductivity decreased. This last effect is certainly related to the phenomenon observed by electron microscopy.

In terms of interpretation model, this Ni segregation, as a localized effect, should not be treated by the brick-layer model, which assumes a homogeneous microstructure. Preferably, the analysis of impedance spectroscopy data was carried out using the blocking factor α_R, given by [12]:

$$\alpha_R = \frac{R_{gb}}{R_g + R_{gb}} \tag{1}$$

where R_g and R_{gb} are the grain and grain boundary resistances, respectively. This dimensionless factor varies with temperature and grain size.

This dimensionless parameter gives an evaluation of the negative effects of any microstructure defects on the electrical conductivity of the material. It has been applied to characterize pores, local cracks, impurity inclusions and less-conductivity
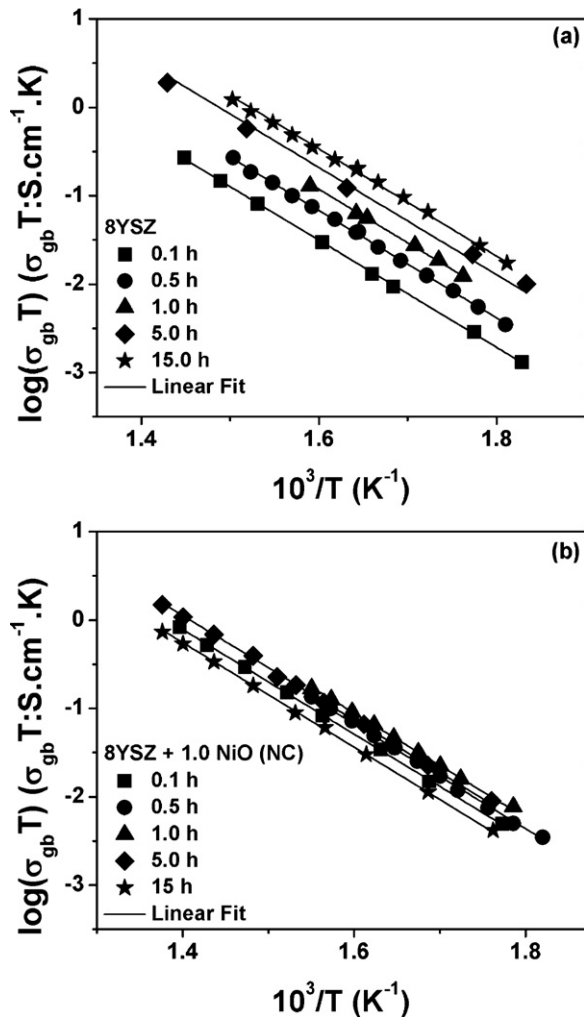
Fig. 9. Arrhenius plots of the grain boundary conductivity corrected for the grain size of 1.0 mol% NiO specimens sintered at several holding times at 1350 °C.

The blocking factor decreases steeply up to 1 h due to pore elimination and densification. For larger holding times α_R decreases slowly for pure 8YSZ and increases for NiO containing specimens. This further decrease of the blocking factor for pure 8YSZ is related to the grain growth, which is the dominant mechanism operating in the last stage of sintering. For specimens containing NiO, the increase in the blocking factor varies with the additive content. Therefore, in specimens containing NiO two mechanisms operate simultaneously in the last stage of sintering: grain growth and nickel segregation. The former decreases α_R, whereas the later has the opposite effect, being dominant.

Fig. 9 shows Arrhenius plots of the grain boundary conductivity for 1.0 mol% NiO specimens sintered at several holding times after correction for the grain boundary surface, according to Miyayama et al. [17].

It is clearly seen that up to 1 h holding time, the grain boundary conductivity does not change with the grain size G (which is inversely proportional to the grain boundary surface). In contrast, grain growth can not account for the observed decrease in the grain boundary conductivity for larger holding times.

These results on electrical conductivity are an evidence that Ni segregation at high temperatures produces a blocking effect, thereby degradation of the grain boundary conductivity of NiO containing 8YSZ specimens occurs. In SOFC anodes, the degradation of the electrical conductivity may change the long-term stability of the device. Although in this case Ni and not NiO is present, nickel segregation is expected to occur as well. In a previous study on anode degradation it was shown that at the anode/solid electrolyte interface a comparative large amount of a secondary phase (silicate-based phase) was present when impure nickel precursor was employed. In addition, even with relatively pure precursor materials, about 1 wt.% of Ni was found at the interface, whereas regions away from the interface were free of Ni [18]. In contrast, for applications at low temperature, small additions of NiO may be

Fig. 7. Arrhenius plots for the grain boundary conductivity of (a) 8YSZ and (b) 8YSZ containing 1 mol% NiO as a function of the holding time at 1350 °C.

phases originating from phase transitions or impurity precipitation [12–16].

Fig. 8 shows the evolution of the blocking factor with the holding time for pure 8YSZ and NiO containing 8YSZ specimens.
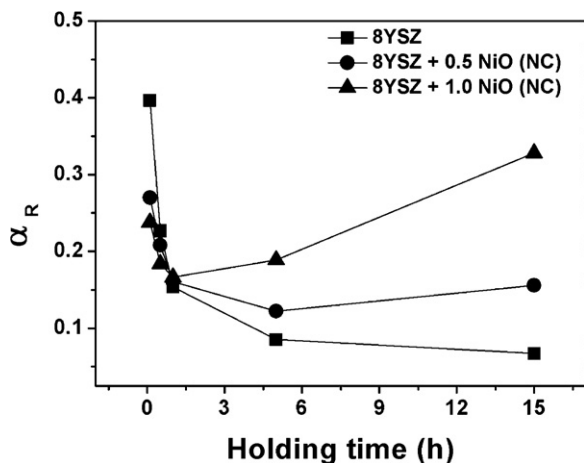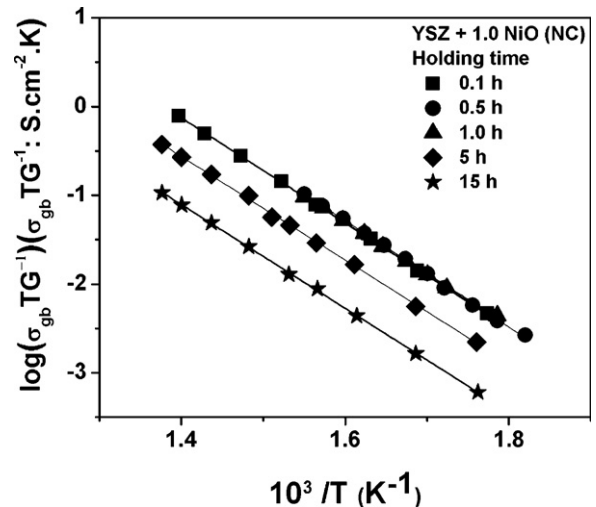

Fig. 8. Evolution of the blocking factor with the holding time at 1350 °C for 8YSZ and NiO containing 8YSZ specimens.

beneficial, because of the improved densification of the material without any significant change of the electrical conductivity.

4. Conclusions

X-ray diffraction data show that the solubility limit of NiO at a typical sintering temperature of 1350 °C is 1.5 mol%. Grain growth and residual porosity elimination are the main microstructure features observed in pure 8YSZ with holding time at 1350 °C. In specimens containing NiO, segregation of the additive occurred for larger holding times ($\geq$5 h) at the sintering temperature.

No differences were observed in the overall electrolyte conductivity when NiO was used as precursor material. The apparent activation energy determined by impedance spectroscopy is 1.12 ± 0.03 eV. Similarly, the grain conductivity is not influenced by small amounts (below the solubility limit) of the additive.

In contrast, a significant blocking effect of charge carriers at grain boundaries was found due to Ni segregation with increasing holding times at 1350 °C.

Acknowledgements

References

[1] S.C. Singhal, Advances in solid oxide fuel cell technology, Solid State Ionics 135 (2000) 305–313.

[2] J.W. Fergus, Electrolytes for solid oxide fuel cells, J. Power Sources 162 (2006) 30–40.

[3] A. Kuzjukevics, S. Linderoth, Interaction of NiO with yttria-stabilized zirconia, Solid State Ionics 93 (1997) 255–261.

[4] P. Shen, S. Chen, H.S. Liu, Annealing-induced defect clustering at $Ni_{1-x}O$-Y-partially-stabilized ZrO_2 interfaces, Mater. Sci. Eng. A161 (1993) 135–143.

[5] A. Kuzjukevics, S. Linderoth, Influence of NiO on phase stabilization in 6 mol% yttria-stabilized zirconia, Mater. Sci. Eng. A232 (1997) 163–167.

[6] S. Linderoth, N. Bonanos, K.V. Jensen, J.B. Bilde-Sorensen, Effect of NiO-to-Ni transformation and structure of yttria-stabilized zirconia, J. Am. Ceram. Soc. 84 (2001) 2652–2656.

[7] J. van Herle, R. Vasquez, Conductivity of Mn and Ni-doped stabilized zirconia electrolyte, J. Eur. Ceram. Soc. 24 (2004) 1177–1180.

[8] W.G. Coors, J.R. O'Brien, J.T. White, Conductivity degradation of NiO-containing 8YSZ and 10YSZ electrolyte during reduction, Solid State Ionics 180 (2009) 246–251.

[9] A.J.C. Wilson, Geiger-counter X-ray spectrometer-influence of size and absorption coefficient of specimens on position and shape of powder diffraction maxima, J. Sci. Instrum. 27 (1950) 321–325.

[10] R.M. Batista, E.N.S. Muccillo, Densification and electrical conductivity of yttria-stabilized zirconia containing NiO additions, ECS Trans. 13 (26) (2008) 47–54.

[11] R.M. Batista, E.N.S. Muccillo, Densification and grain growth of 8YSZ containing NiO, Ceram. Int. 37 (2011) 1047–1053.

[12] M. Kleitz, H. Bernard, E. Fernandez, E. Schouler, Advances in Ceramics, in: A.H. Heuer, L.W. Hobbs (Eds.), Science and Technology of Zirconia I, v. 3, The American Ceramic Society, Columbus, OH, 1981 pp. 310–336.

[13] L. Dessemond, R. Muccillo, M. Hénault, M. Kleitz, Electric conduction-blocking effects of voids and second phases in stabilized zirconia, App. Phys. A57 (1993) 57–60.

[14] M. Kleitz, L. Dessemond, M.C. Steil, Model for ion-blocking at internal interfaces in zirconias, Solid State Ionics 75 (1995) 107–115.

[15] E.N.S. Muccillo, M. Kleitz, Impedance spectroscopy of Mg-partially stabilized zirconia and cubic phase decomposition, J. Eur. Ceram. Soc. 16 (1996) 453–465.

[16] M.C. Steil, F. Thevenot, K. Kleitz, Densification of yttria-stabilized zirconia - impedance spectroscopy analysis, J. Electrochem. soc. 144 (1997) 390–398.

[17] M. Miyayama, H. Inoue, H. Yanagida, Grain-boundary resistivity of stabilized zirconia films, J. Am. Ceram. Soc. 66 (1983) C164–166.

[18] Y.L. Liu, S. Primdahl, M. Mogensen, Effects of impurities in Ni/YSZ-YSZ half-cells for SOFC, Solid State Ionics 161 (2001) 1–10.